

KCl-Induced High-Temperature Corrosion Behavior of HVAF-Sprayed Ni-Based Coatings in Ambient Air

Reza Jafari¹ · Esmail Sadeghimeresht² · Taghi Shahrabi Farahani¹ ·
Matti Huhtakangas³ · Nicolaie Markocsan² · Shrikant Joshi²

Submitted: 26 July 2017 / in revised form: 12 December 2017 / Published online: 2 January 2018
© The Author(s) 2017. This article is an open access publication

Abstract KCl-induced high-temperature corrosion behavior of four HVAF-sprayed Ni-based coatings (Ni21Cr, Ni5Al, Ni21Cr7Al1Y and Ni21Cr9Mo) under KCl deposit has been investigated in ambient air at 600 °C up to 168 h. The coatings were deposited onto 16Mo3 steel—a widely used boiler tube material. Uncoated substrate, 304L and Sanicro 25 were used as reference materials in the test environment. SEM/EDS and XRD techniques were utilized to characterize the as-sprayed and exposed samples. The results showed that the small addition of KCl significantly accelerated degradation to the coatings. All coatings provided better corrosion resistance compared to the reference materials. The alumina-forming Ni5Al coating under KCl deposit was capable of forming a more protective oxide scale compared to the chromia-forming coatings as penetration of Cl through diffusion paths was hindered. Both active corrosion and chromate formation mechanisms were found to be responsible for the corrosion damages. The corrosion resistance of the coatings based on the microstructure analysis and kinetics had the following

ranking (from the best to worst): Ni5Al > Ni21Cr > Ni21Cr7Al1Y > Ni21Cr9Mo.

Keywords biomass boiler · Cl-induced corrosion · high-temperature corrosion protection · high-velocity air–fuel (HVAF) · Ni-based coatings

Introduction

In recent decades, biomass and waste fuels are being increasingly used as renewable and CO₂-free resources of energy in power generation industry (Ref 1). High-temperature gases resulting from the combustion of such fuels often contain chlorine compounds which may deposit on degradation-prone parts of boilers, in particular the superheater tubes. This leads to a harsh environment that is highly corrosive to the tube materials (Ref 2). Demands for higher energy production efficiency lead to an increase in operational temperature, which may accelerate corrosion damages even to high corrosion resistance materials (Ref 3). Alkali chloride/chlorine accelerates corrosion by reacting with protective metal oxide scale via the “active oxidation” mechanism (Ref 4–8), resulting in internal attack, formation of defects and non-adherent scale, accordingly material degradation. Besides, transformation of the protective chromia scale into chromate is reported as another mechanism (“chromate formation” mechanism) leading to depletion of Cr and breakdown of the protective scale (Ref 9–11). According to the literature concerning the effect of biomass fuels on corrosion mechanisms, KCl is found to be the dominant component of the deposit near the metal surface which plays a key role in Cl-induced corrosion problems faced by many power plants (Ref 6, 12).

This article is an invited paper selected from presentations at the 2017 International Thermal Spray Conference, held June 7–9, 2017, in Düsseldorf, Germany, that has been expanded from the original presentation.

✉ Esmail Sadeghimeresht
esmaeil.sadeghimeresht@hv.se; sadeghimeresht@hv.se

Taghi Shahrabi Farahani
tshahrabi34@modares.ac.ir

¹ Department of Material Science and Engineering, Tarbiat Modares University, Tehran 14115-143, Iran

² Department of Engineering Science, University West, 461 53 Trollhättan, Sweden

³ M. H. Engineering AB, 691 42 Karlskoga, Sweden

In order to control the corrosion damages, utilization of highly alloyed Ni-based components instead of traditional low alloy steels has been proposed (Ref 13, 14). However, developing more noble materials is not always practically and economically favorable (Ref 15). Flexibility of coating technologies allows manufacturing of dense and highly adherent coatings which can meet the critical protection requirements of such a boiler environment. The rapid development of thermal spray processes offers attractive and cost-effective routes to avoid degradation of low alloy tubes by selecting appropriate coating chemistry and manufacturing process (Ref 16, 17). A variety of thermal spray methods including atmospheric plasma spray (APS), arc spray and high-velocity air–fuel (HVOF) have been already used to fabricate corrosion resistant coatings (Ref 18–22). High-velocity air–fuel (HVAF), a promising method to produce dense and adherent coating, works based on high-velocity impact of molten or semi-molten particles which could be used to apply a wide range of coating materials including Ni-based powders (Ref 23–26). Recent advances in design and development of new HVAF guns have reduced the cost and enhanced the quality of coatings, resulting in booming markets for HVAF technology (Ref 27–29). The coatings produced by HVAF, characterized by lower porosity, less in situ formed oxide content and more interlamellar cohesion, are capable of reducing the diffusion of aggressive agents such as chlorine toward substrate/coating interface (Ref 30, 31). The few studies performed on HVAF-sprayed Ni-based coatings showed that the coatings presented excellent oxidation behavior in oxidizing environments (Ref 32). However, the corrosion mechanisms of such coatings in oxidizing–chloridizing environment need to be studied further from both thermodynamics and kinetics point of view.

In the present study, high-temperature corrosion behavior of four commercially available Ni-based coatings—Ni21Cr, Ni5Al, Ni21Cr9Mo and Ni21Cr7Al1Y (all compositions in wt.%)—sprayed by HVAF was investigated in a simplified oxidizing–chloridizing boiler environment to assess the effect of KCl. The selection of the feedstock powders was based on the presence of beneficial alloying elements, i.e., Al and/or Cr which play key roles in formation of protective alumina and chromia scales in an aggressive chlorine environment (Ref 33).

Experimental Details

Materials

Three commercially available Ni-based powders of Ni21Cr-Amperit 251.001, Ni5Al-Amperit 281.003 and Ni21Cr7Al1Y-Amperit 413.001 sourced from H.C Starck

GmbH (Germany), as well as a proprietary SiO₂-containing Ni21Cr9Mo formulation supplied by M.H. Engineering AB (Sweden), were used as feedstock powders. SiO₂ was intentionally added in case of the last powder in an effort to provide enhanced high-temperature corrosion resistance. 16Mo3, a low alloy ferritic steel commonly used in fabrication of boiler parts, was selected as the substrate material for coatings and as a reference material. Specimens of 304L and Sanicro 25 (prepared from conventional boiler tubes) by cutting to the segments were used as reference materials, due to their extensive use in high-temperature applications. The KCl salt, with particle size of 45–155 μm, was used as the chlorine-containing deposit.

Spray Method and Sample Preparation

A HVAF gun (Uniquecoat M3TM, Oilville, VA, USA) was utilized to spray the coatings. The 16Mo3 rods (Diameter = 25 mm and length = 500 mm) were fixed in a horizontal rotating mandrel for applying the coating on the cylindrical surface. After spraying, the rod was cut into pieces of 5 mm length and coatings were applied on both the flat faces to ensure that the specimens were coated on all sides. The substrates were grit blasted by alumina grits (mesh 220) prior to spraying for cleaning and roughening the surfaces. Several combinations of thermal spray parameters were initially tried and the resulting coatings characterized to determine spray conditions that yielded least porosity. The selected process parameters are presented in Table 1. All coatings were sprayed to a thickness of ~ 250 μm and then ground to a 1500-grit SiC paper and polished using a 0.3-μm alumina suspension to unify the effect of surface roughness for all coatings.

High-Temperature Corrosion Test

All samples were weighed, and dimensions were recorded by a digital micrometer before KCl deposition. KCl dissolved in an ethanol/water mixture was sprayed on the samples to form 0.1 mg/cm² deposit. Isothermal high-temperature corrosion test was performed at 600 °C in an air furnace up to 168 h. The temperature was raised at 10 °C/min, and after the high-temperature test, the specimens were cooled down in the furnace to 200 °C. To diminish the shielding effect, the samples were placed next to each other with a distance of around 50 mm. Afterward, the tested samples were extracted from the furnace and cooled down to room temperature. All tested samples were weighed after removing residual KCl particles. The corrosion performance of the coatings is subsequently discussed in relation to microstructure, phase formation and noted mass change, in comparison with reference materials exposed to the same conditions. All samples were kept in a

Table 1 HVAF spray process parameters

Variables	NiCr	NiAl	NiCrMo	NiCrAlY
Nozzle type	4L2G	4L4G	3L2G	4L2G
Fuel 1 (propane) pressure, MPa	0.7	0.7	0.7	0.7
Fuel 2 (propane) pressure, MPa	0.7	0.7	0.8	0.7
Carrier gas (N ₂) pressure, MPa	0.4	0.4	0.4	0.4
Feed rate, g/min	150	150	150	150
Stand-off distance, mm	300	300	300	300
Pass velocity, m/min	50	50	50	50

desiccator with silica gel prior to and after high-temperature exposure until post-analysis had been conducted.

Characterization of Powders and Samples Before and After Exposure

The powders' and coatings' morphology, and cross section before and after the exposures were studied using a TESCAN VEGAII scanning electron microscope (SEM) equipped with a RONTEC QUANTAX-Q2 energy dispersive spectroscopy (EDS) system. Mass changes after exposure were recorded to study the corrosion kinetics of the coatings in comparison with the substrate and reference materials. The phase composition of the as-received powders, and also the as-sprayed and exposed coatings, was determined by a Philips-PW1730 x-ray diffractometer (XRD; Cu target with $\lambda = 0.154$ nm) over a 2θ range of 10° – 80° . Samples cold mounted in a low shrinkage cast resin were cut by a low speed saw prior to metallographic preparation. Cross-sectional analysis was performed to investigate the coatings' features and corrosion performance. ImageJ, an open access image analyzer software, was used to measure coatings' porosity in precisely prepared metallographic cross sections.

Results and Discussion

Characterization of Coatings and Feedstock Powders

Figure 1 shows the spherical or near-spherical morphology of the feedstock powders. The Ni₂₁Cr₉Mo powder showed more homogeneity in size distribution than the other feedstock powders. Cross-sectional SEM images of as-sprayed coatings taken in BSE mode (Fig. 1) exhibited almost dense and defect-free coatings for all compositions. This suggested that the semi-molten particles sufficiently deformed upon impact with the substrate or/and previously deposited layers. Good interlocking at the substrate/coating interface, well-adhered splats and low porosity content were evidence of proper parameter selection and HVAF

potential for manufacturing dense and uniform coatings (Ref 30). Table 2 provides a summary of the coatings' properties.

Very minimal phase change was found between the as-sprayed coatings and the starting feedstock powders, as evident from the XRD patterns illustrated in Fig. 2. No feedstock oxidation and/or elemental loss related to the spray method was observed. This was in contrast to the phase change previously reported in the HVOF deposition of Ni-based powders (Ref 34, 35) and represented a specific advantage of the HVAF technique, characterized by lower temperatures and higher particle velocities. Thus, the good interlamellar cohesion discussed in [Characterization of Coatings and Feedstock Powders](#) section could be also attributed to the lower oxidation state of the splashed particles during the spray process.

Corrosion Test Results

Mass Changes and Corrosion Layer Measurement

In order to evaluate the corrosion resistance of the coatings, the mass changes of the samples were measured following exposures, after removing the residual deposited salts. Ni₂₁Cr and Ni₅Al showed less change in mass as an indication of better performance in comparison with the other coatings and reference materials (see Fig. 3). However, the change in mass is not a reliable parameter to calculate the exact corrosion rate and it is just valid for a comparison among the samples tested in this study. Surface reactions that involve deposit and alloying elements, over/under deposit cleaning after the high-temperature corrosion test, internal corrosion damages and formation of volatile compounds can be sources of inaccuracy in mass change measurements.

Figure 3 also reveals lower corrosion degradation of coatings by comparing the median value of formed scale thickness, defined as thickness of general corrosion products on each coating cross section. Internal corrosion and spallation were not considered in the calculations. In most cases, the corrosion layer thickness was in a good accordance with the observed mass gains. It should be noted that

Fig. 1 SEM secondary electron mode (SE) images of the powder feedstocks and cross-sectional backscattered electron (BSE) images of Ni-based HVAF as-sprayed coatings, (a) Ni21Cr, (b) Ni21Cr7Al1Y, (c) Ni5Al and (d) Ni21Cr9Mo

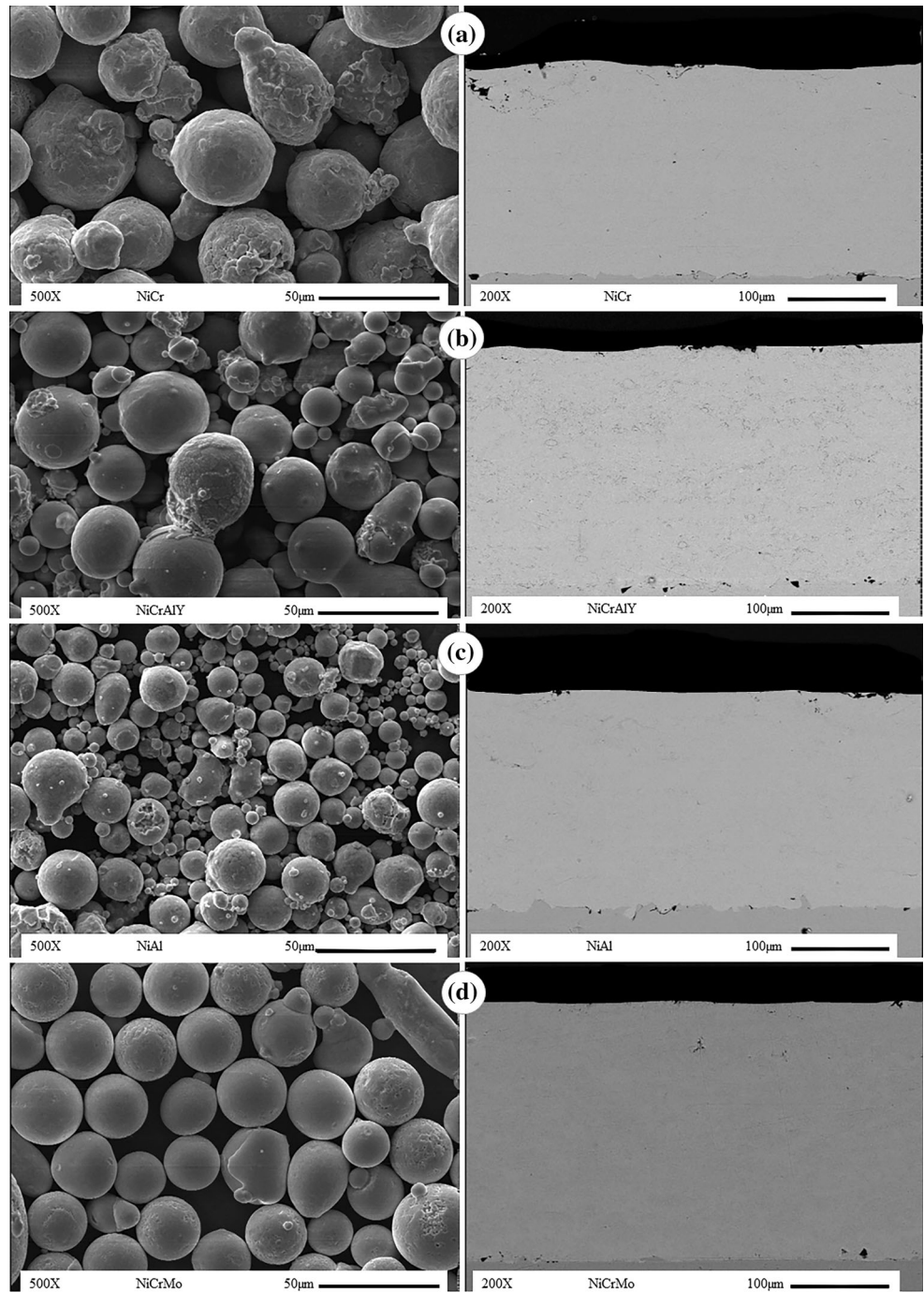


Table 2 Summary of coating properties

Materials	Coating thickness, μm^{a}	Coating roughness, R_{a} , μm^{b}	Coating porosity, vol. %
NiCr	221 ± 21	< 0.1	0.4 ± 0.02
NiAl	235 ± 12	< 0.1	0.3 ± 0.07
NiCrAlY	236 ± 24	< 0.1	0.5 ± 0.10
NiCrMo	218 ± 7	< 0.1	0.3 ± 0.09

^aAverage of 20 individual measurements

^bAverage of 3 individual measurements on 2 directions

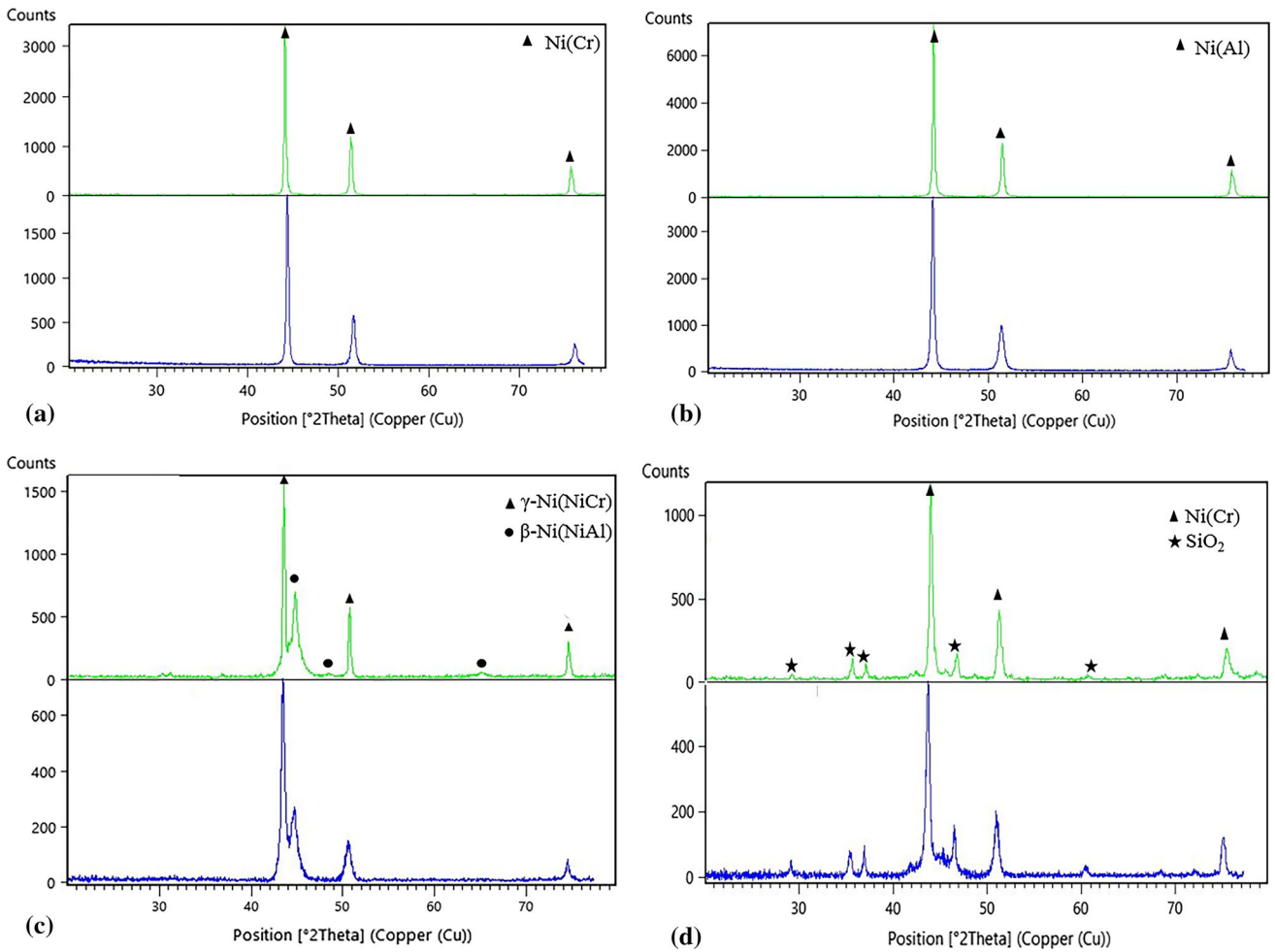
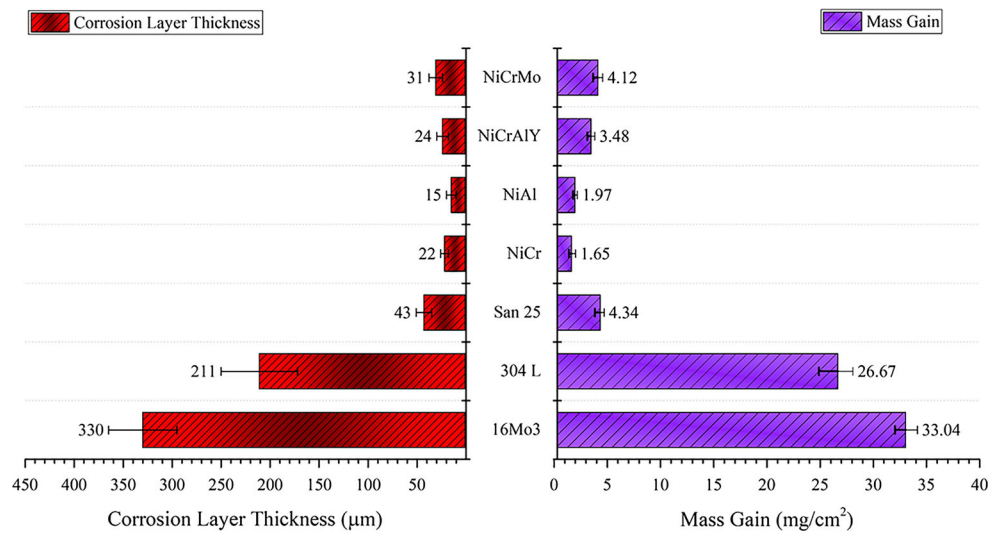


Fig. 2 XRD pattern of powder feedstocks (upper) and as-sprayed coatings (lower) limited to 20°–80°. (a) Ni₂₁Cr, (b) Ni₅Al, (c) Ni₂₁Cr₇Al₁Y, and (d) Ni₂₁Cr₉Mo

Fig. 3 Thickness of the formed scale (average of 10 measurements) and mass gain of the samples exposed to KCl deposit at 600 °C for 168 h



corrosion protection is expected from dense and slow growing oxide scales (Ref 22). The standard deviation of measurements, shown as error bars in Fig. 3, was a measure of variation in corrosion layer thickness along the studied coating cross sections.

Visual Observation of Samples After High-Temperature Corrosion Test

Dark gray as-sprayed samples turned to shiny metallic color after grinding/polishing. An obvious change in the specimens' appearance, including color change, and localized coating spallation was observed after 168 h exposure at 600 °C under KCl (Fig. 4). The reference materials showed more noticeable changes especially in the form of wide cracks, substantial spallation and swelling of scales, verifying that there was no protection from the formed oxide scales. The substrate material (16Mo3) showed no protection in the test environment, as the corrosion products peeled off from the sample during the mass change measurement.

Microstructural Characterization of Exposed Coated Samples

Figure 5 shows the typical surface morphologies of the Ni-based coatings exposed under KCl at 600 °C, which were markedly different in composition and topography from each other. Figure 5(a) and (b) shows more compacted scales for Ni21Cr and Ni5Al, respectively, in comparison with Fig. 5(c) (Ni21Cr7Al1Y) and (d) (Ni21Cr9Mo). The EDS data derived from exposed surface of Ni5Al revealed that the scale mainly consisted Ni, O, Al, a small amount of Cl (< 2 wt.%) and K (< 1 wt.%), while no Cl was detected in Ni-, Cr- and O-rich oxide layer formed on the surface of exposed Ni21Cr.

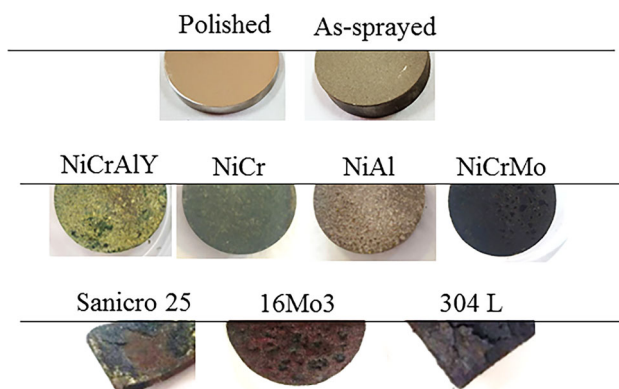


Fig. 4 Visual observation of the coatings and the reference samples after the exposure to KCl at 600 °C for 168 h. Significant spallation and degradation of reference materials compared to coated samples is noticeable

Less compacted and platelet-shaped chromium-rich scale on Ni21Cr7Al1Y outer surface shown in (Fig. 5c) could give an explanation of the coating degradation under the test condition. The oxide scale on Ni21Cr9Mo also contained K, probably in spinel form. In particular, some cracks found in the oxide scale on Ni21Cr9Mo (Fig. 5d) could act as penetration path for corrosive agents. The Ni21Cr9Mo coating contained SiO₂; however, no clear sign of Si was observed on the surface of the formed oxide, confirming no contribution of Si in the oxide scale. As reported in the literature (Ref 36), SiO₂ affects the oxidation mechanism by acting as nucleation sites for the protective oxide layer to be formed on the surface. The role of SiO₂ in increasing the corrosion resistance of the coatings in the oxidizing–chloridizing will be thoroughly investigated in a separate paper.

Figure 6 shows the cross section of exposed samples after the exposure. The growth of the formed oxide layer varied in thickness which could be responsible for reducing the diffusion of Cl and O through the coating. In spite of the continuous scale formed on Ni21Cr, the oxidizing agents found their paths through boundaries between splats to the coating midsection (Fig. 6a). Ni21Cr suffered from corrosion through intersplat boundaries such that one could see the oxidized regions at the middle of coating in Fig. 6(a). In the contrary, Ni21Cr9Mo preserved its interlamellar cohesion in such that neither visible splat boundaries nor corrosive agents were observed through the coating (Fig. 6d). Similar behavior was seen for the Ni5Al sample (Fig. 6b). There were seemingly more cracks in the Ni21Cr7Al1Y coating after exposure (Fig. 6c), compared to the other coatings in Fig. 6. It should be noted that remarkable voids existed in the thick scale formed on Ni21Cr9Mo followed by microcracks parallel to the coating distinguished the scale structure from the other coatings.

More details from corrosion behavior of subjected coatings could be studied from distribution of major constituent elements. X-ray elemental map images taken from coated sample cross sections after high-temperature corrosion test are shown in Fig. 7. Clear depletion of Ni did not occur in the examined cross sections, but Ni participated in formation of the oxide scale especially in Ni21Cr9Mo. Moderate oxide scale formed on Ni21Cr, which mainly contained Ni, Cr and O in oxide layer, and Cr was depleted under oxide layer to roughly 40 μm depth in (Fig. 7a). On the other hand, internal attacks severely affected the Ni21Cr coating outermost region, adjacent to the corrosion scale visible in Fig. 7(a). Cl accumulation confirmed the penetration of Cl through the Ni21Cr coating.

In case of Ni5Al, Al clearly migrated to the coating's top surface, formed alumina and left the coating behind

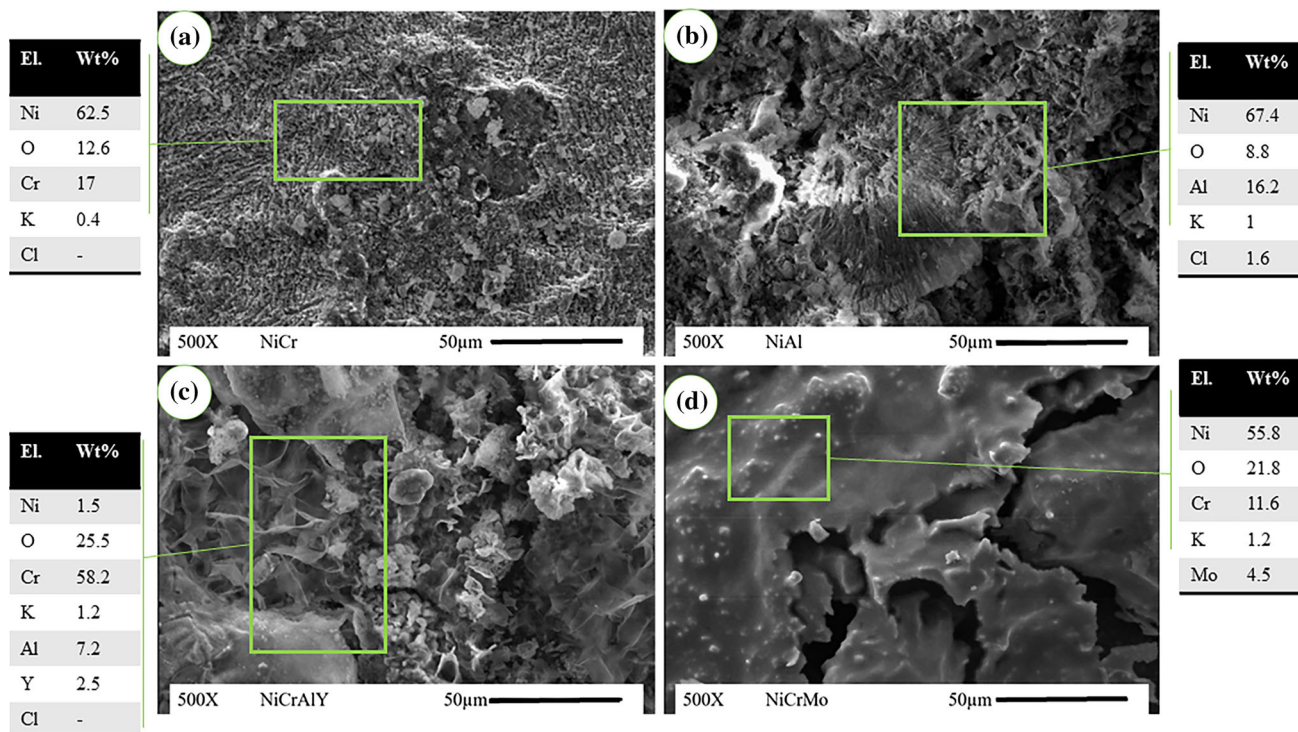


Fig. 5 Surface morphology of coated samples after high-temperature corrosion tests. (a) Ni21Cr, (b) Ni5Al, (c) Ni21Cr7Al1Y and (d) Ni21Cr9Mo

depleted in Al. The elemental mapping micrographs indicated that formed scale consisted O and Al. Hence, the penetration paths of Cl and O through the coatings were blocked and considerable portion of the coating remained immune from corrosion. Apparently, Cl entrapped in Ni5Al oxide scale (Fig. 6b and 7b). It might be suggested that in the initial stages of high-temperature exposure, Cl diffused inward through the scale and reacted with alloying elements, while outward diffusion occurred slowly or completely hindered in accordance with the active oxidation and blanketing effects (Ref 5, 14, 37).

On the contrary to the Ni5Al coating, Ni21Cr9Mo had a thick oxide scale including Ni, Cr, K and O according to the EDS results which probably led to formation of spinel oxide (Fig. 7d). However, there is no clear evidence for penetration of Cl through the coating. In spite of the thick and defected scale which indicate less corrosion resistance, the corrosion reaction seemed to have continued under the scale uniformly as there were no signs of localized elemental depletion and corrosion products in splat boundaries. It may originate from good interlamellar adhesion and less connected path through the coating which left no way for intensive localized corrosion by penetrations of the corrosive agents.

The Cr depletion in Fig. 7(c) occurred in a wide range up to about 70 µm from the coating's top surface. It seems that no continuous protective scale formed on

Ni21Cr7Al1Y or the formed scale possibly spalled during exposure. As a consequence, the coating encountered internal corrosion attack, despite the presence of Al and Cr more than the other coatings.

The integrity of the coating/substrate contact remained sound even after corrosion testing in most of the coatings. However, it should be noticed that coatings which suffered from continuous cracks (e.g., Ni21Cr7Al1Y) were unable to provide corrosion protection in the current test condition even if excellent corrosion resistance was expected from microstructure studies. If the chlorine and oxygen-containing products reach the cracks and diffuse to the coating/substrate interface, formation of brittle and massive phases is the negative drawback which may lead to coating's detachment.

Phase Constituent of the Exposed Coatings

The XRD patterns of corroded samples shown in Fig. 8 indicated presence of oxides and spinel structures, e.g., NiCr₂O₄ that formed in a reaction between NiO and Cr₂O₃ (Ref 38). Transition metal chlorides, e.g., NiCl₂, NiCl₃ or CrCl_x peaks, were not observed in XRD spectra in Fig. 8(a) and (b) probably due to higher amount of the stable and protective oxides, e.g., Cr₂O₃ and Al₂O₃ and XRD detection limit. Formation of NiCl₂ is supported by the XRD patterns in Ni21Cr7Al1Y, seen in Fig. 8(c) which

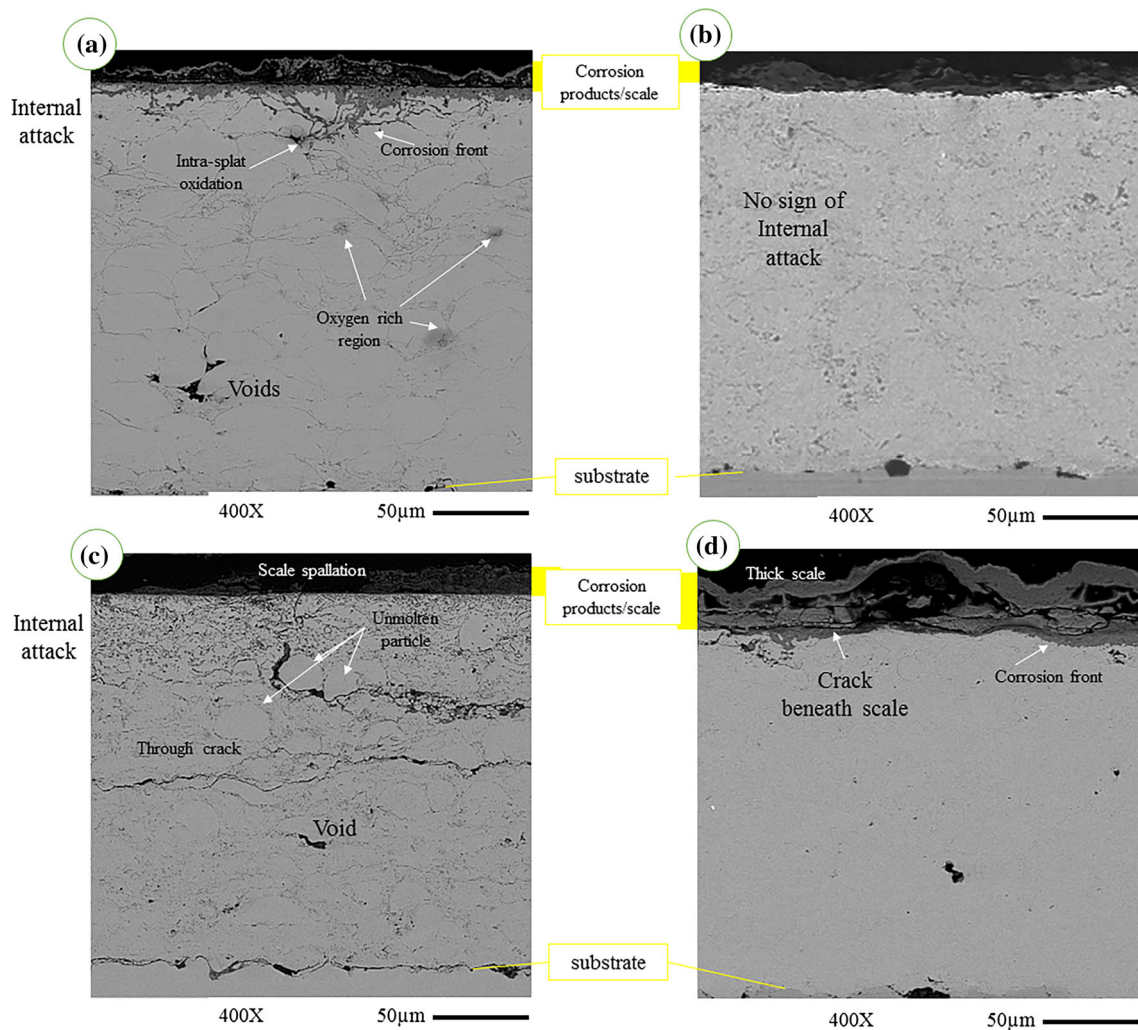


Fig. 6 Cross-sectional BSE overview images of coated samples exposed to deposited KCl at 600 °C for 168 h. (a) Ni21Cr, (b) Ni5Al, (c) Ni21Cr7Al1Y and (d) Ni21Cr9Mo

corresponded to the coating that was unable to form a continuous and protective scale. These findings were in a good accordance with studies concerning active oxidation mechanism (Ref 5, 22). XRD spectra peaks attributable to KCr_2O_4 were also observed in case of exposed Ni21Cr9Mo coatings, corroborating the earlier observation from the elemental map that K (without Cl) remained in addition to Cr at the Ni21Cr9Mo surface. It should be noted that formation of K_2CrO_4 previously reported as a destructive factor in the breakaway of the protective oxide scale which leaves behind a thick and permeable scale (Ref 10). As shown by topography EDS data in Fig. 5(d), Mo was detected on the Ni21Cr9Mo surface. Evidently, XRD results (Fig. 8d) confirmed the formation of MoO_3 as another phase constituent which was not supposed to resist against corrosive attacks in oxidizing–chlorinating environment (Ref 33).

In the previous work using the similar coating's composition exposed in ambient air (Ref 32), there were signals of SiO_2 in the Ni21Cr9Mo coating (which were mistakenly labeled as MoO_3 and Cr_2O_3), most probably due to the formation of a thin oxide scale on the surface. As the formed oxide scale was thin, the XRD peaks observed were mostly from the background (Ni21Cr9Mo coating which contained SiO_2). It seems that the beneficial effect of SiO_2 on oxidation mechanism would perhaps be obvious in more aggressive environments, and this is the subject of an ongoing study which will be reported in a separate paper.

Corrosion Behavior of Coatings

Chlorine is able to penetrate through the defected and poorly protective oxide scales along cracks and reacts with the coating's or substrate's elements such as Cr to form metallic chlorides where there is a poor access to oxygen

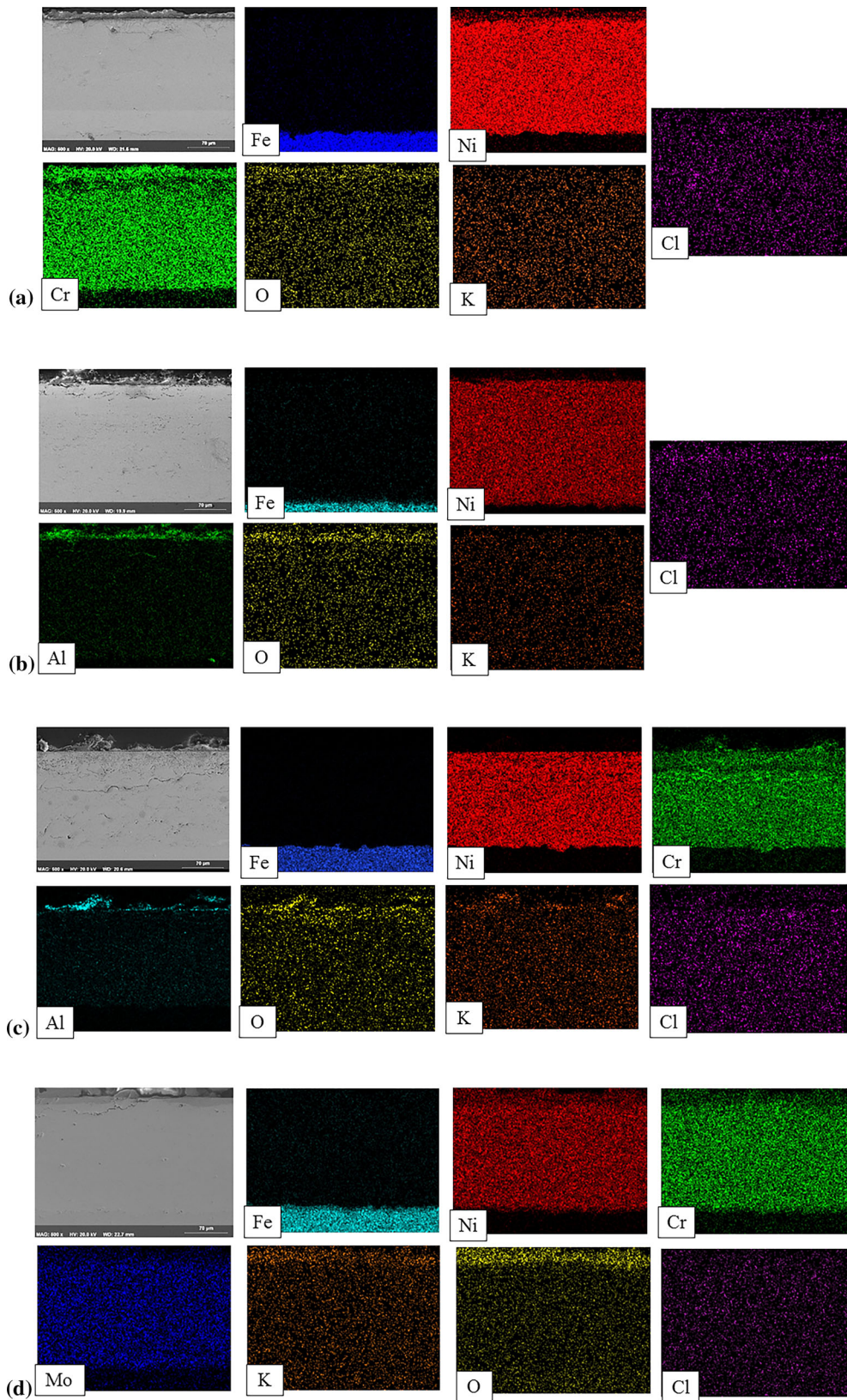


Fig. 7 X-ray elemental map micrographs taken from cross section of coated samples exposed under KCl at 600 °C for 168 h. (a) Ni₂₁Cr, (b) Ni₅Al, (c) NiCrAlY and (d) Ni₂₁Cr₉Mo

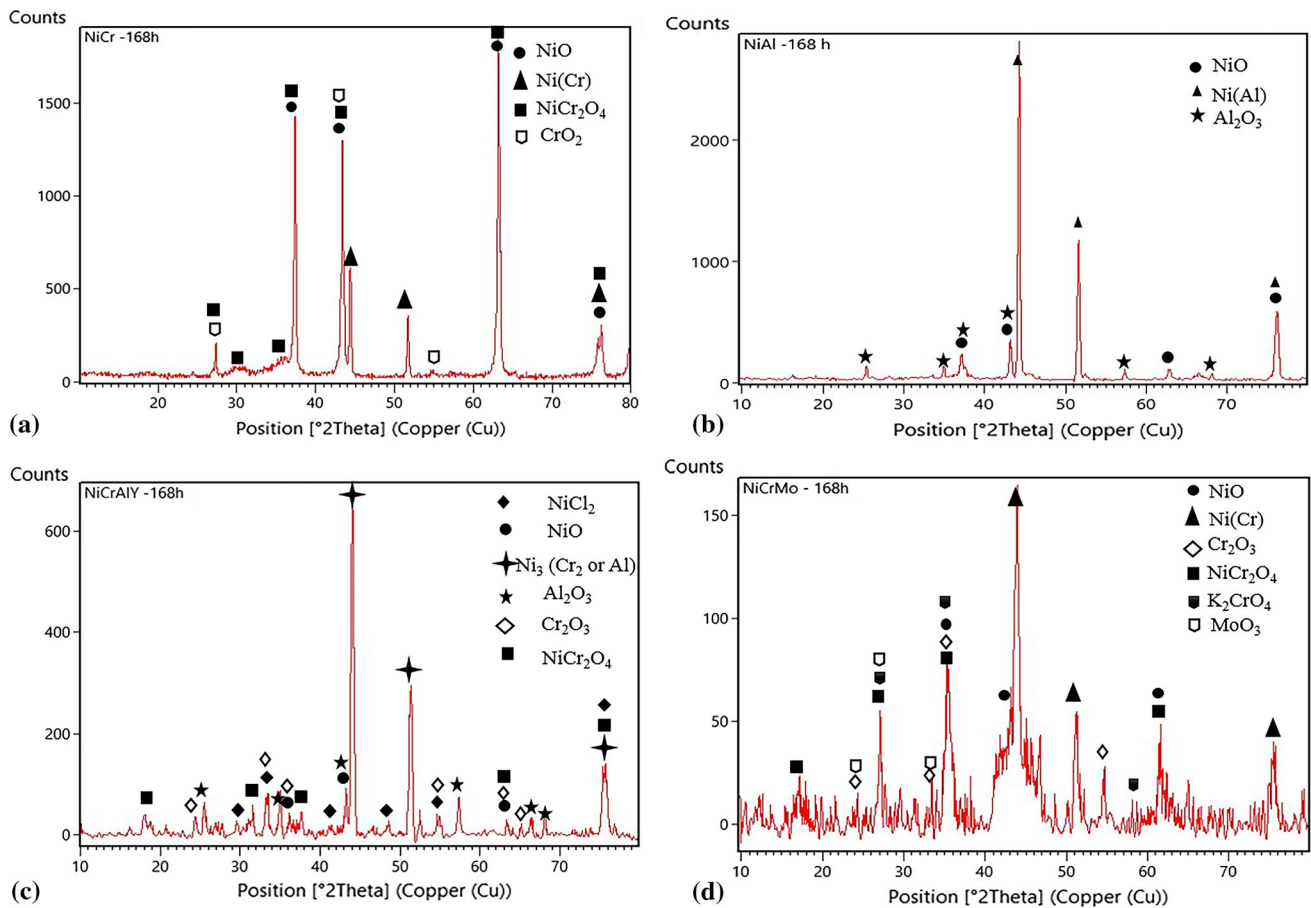


Fig. 8 XRD patterns and identified phases of coatings after high-temperature corrosion after 168 h. (a) Ni21Cr, (b) Ni5Al, (c) Ni21Cr7Al1Y and (d) Ni21Cr9Mo

(low oxygen partial pressure). By increasing p_{Cl_2} and decreasing p_{O_2} beneath the formed oxide layer, formation of volatile chlorides is thermodynamically favored compared to formation of oxides in such locations (Ref 8, 33). The volatile chlorides tend to transfer outward through the diffusion paths toward the coating surface. These chlorides convert to oxides where oxygen is more available (higher oxygen partial pressure), resulting in a porous oxide scale (Ref 22). In an oxidizing–chloridizing environment, the competition is between Cl and O, depending on the alloying elements. Rather slow growth of the oxide layer formed on Ni5Al enhanced the corrosion protection by a thinner scale (see Fig. 3). In contrast, higher thickness of the poor quality scales in case of the other coatings was responsible for a much higher degree of corrosion. The performance of presently investigated Ni-based coatings in pure oxidation environment was previously evaluated (Ref 32). Ni21Cr7Al1Y was found to impart superior oxidation resistance compared to the other coatings as well as Sani-cro 25. In the current work, oxidation was intensively accelerated in presence of KCl deposit for all tested materials, especially Ni21Cr7Al1Y. Cross-sectional studies

were in a good agreement with thermogravimetric measurements in most cases. The noted deviation in Ni21Cr results may originate from complexity associated with simultaneous oxide formation and internal degradation within the coating followed by evaporation of volatile chlorides. Besides, removing the KCl particles which could face oxide overgrown (Ref 39) could be another source for the result mismatch.

In the initial stage, splat boundaries adjacent to the KCl deposit can sometimes provide feasible diffusion paths for corrosive agents toward the metal surface. Depending upon the coating chemistry, the kinetics of oxide scale formation and the protection ability of these oxides, massive oxide scales can form at longer exposure and these may peel off, leading to heavy damage to the part in service in cases where continuous scale growth is not always expected.

Considering coating compositions variation, Cr-bearing coatings showed good protection against corrosion in gaseous HCl-oxidizing environment at elevated temperatures (Ref 22), while alkali chloride species could severely damage chromium-rich oxide scale by formation of chromate (Ref 11, 21). From thermodynamics point of view,

alumina has higher stability since KCl and protective oxide reaction is more favorable in case of Cr_2O_3 in comparison with Al_2O_3 (Ref 40).

It is practically confirmed that Al-bearing coatings represent good candidates for protection against alkali chloride species (Ref 41, 42). Ni5Al and Ni21Cr7Al1Y samples are potential alumina-forming coatings among tested materials. Combination of Cr- and Al-rich oxide is supposed to provide a more protective layer at initial corrosion stages. However, protectiveness of oxide scale maintains if only the scale remains integrated (Ref 40, 43). But HVAF-sprayed Ni21Cr7Al1Y failed to provide a continuous and impermeable alumina scale presumably because of test temperature which was not high enough to promote the formation of protective alpha-alumina (Ref 44). Cr-rich oxide was also formed which was known to be susceptible to the chromate formation. In addition, formation of massive compounds and volatile species lead to defected oxide scales similar to the observed conditions in Ni21Cr, Ni21Cr7Al1Y and Ni21Cr9Mo coatings which may cause final complete failure of the coatings.

Voids and oxides formed during the coating process are known to be weak spots in thermally sprayed coatings' performance in chlorine-containing environments (Ref 22). However, as discussed before, the investigated cross sections showed considerably dense coatings, with no oxide content at splat boundaries, although a few semi-molten or unmolten particles were identified in Ni21Cr and Ni21Cr7Al1Y coatings. Considering the coating structure, localized corrosion could be suppressed in the HVAF-sprayed coatings, especially it could be seen in the Ni21Cr9Mo sample with a dense and well-adhered structure.

Conclusion

The HVAF-sprayed Ni-based coatings produced in this study were able to protect the substrates in the alkali chloride-containing environment. In all coatings, the oxide scales covered the sample surfaces, which had different microstructure and density after the exposure to KCl for a week at 600 °C. Chromia-forming materials were prone to degradation by chromate formation, in addition to the active oxidation. Exposed HVAF Ni-based coatings remained attached to the substrate after the test and hindered from the corrosive agents to access the coating/substrate interfaces. Formation of stable Al-rich oxide scale on Ni5Al sample provided an acceptable level of protection, whereas the other coatings affected by corrosion attacks beneath Cr-rich oxide scales. However, all coatings improved high-temperature corrosion resistance in

collation to reference materials from the best to worst as; Ni5Al > Ni21Cr > Ni21Cr7Al1Y > Ni21Cr9Mo.

Acknowledgments Financial support of the Knowledge Foundation (SCoPe: Dnr 20160201) is highly acknowledged. The authors would like to thank Mr. Jonas Olsson, Mr. Stefan Björklund and Mr. Kenneth Andersson for their valuable help and advice in processing and characterization of the HVAF coatings in this study.

Open Access This article is distributed under the terms of the Creative Commons Attribution 4.0 International License (<http://creativecommons.org/licenses/by/4.0/>), which permits unrestricted use, distribution, and reproduction in any medium, provided you give appropriate credit to the original author(s) and the source, provide a link to the Creative Commons license, and indicate if changes were made.

References

1. R. Saidur, E.A.A. Abdelaziz, A. Demirbas, M.S.S. Hossain, and S. Mekhilef, A Review on Biomass as a Fuel for Boilers, *Renew. Sustain. Energy Rev.*, 2011, **15**(5), p 2262-2289
2. N. Otsuka, A Thermodynamic Approach on Vapor-Condensation of Corrosive Salts from Flue Gas on Boiler Tubes in Waste Incinerators, *Corros. Sci.*, 2008, **50**(6), p 1627-1636
3. M. Montgomery, S.A. Jensen, U. Borg, O. Biede, and T. Vilhelmsen, Experiences with High Temperature Corrosion at Straw-Firing Power Plants in Denmark, *Mater. Corros.*, 2011, **62**(7), p 593-605
4. H.J. Grabke, E. Reese, and M. Spiegel, The Effects of Chlorides, Hydrogen Chloride, and Sulfur Dioxide in the Oxidation of Steels Below Deposits, *Corros. Sci.*, 1995, **37**(7), p 1023-1043
5. A. Zahs, M. Spiegel, and H.J.J. Grabke, Chloridation and Oxidation of Iron, Chromium, Nickel and Their Alloys in Chloridizing and Oxidizing Atmospheres at 400-700 °C, *Corros. Sci.*, 2000, **42**(6), p 1093-1122
6. H.P. Nielsen, F.J. Frandsen, K. Dam-Johansen, and L.L. Baxter, Implications of Chlorine-Associated Corrosion on the Operation Of Biomass-Fired Boilers, *Prog. Energy Combust. Sci.*, 2000, **26**(3), p 283-298
7. T. Blomberg, Which are the Right Test Conditions for the Simulation of High Temperature Alkali Corrosion in Biomass Combustion?, *Mater. Corros.*, 2006, **57**(2), p 170-175
8. M. Spiegel, A. Zahs, and H.J. Grabke, Fundamental Aspects of Chlorine Induced Corrosion, *Mater. High Temp.*, 2003, **20**(2), p 153-159
9. T. Jonsson, J. Froitzheim, J. Pettersson, J.E. Svensson, L.G. Johansson, and M. Halvarsson, The Influence of KCl on the Corrosion of an Austenitic Stainless Steel (304L) in Oxidizing Humid Conditions at 600 °C: A Microstructural Study, *Oxid. Met.*, 2009, **72**(3-4), p 213-239
10. C. Pettersson, J. Pettersson, H. Asteman, J.E. Svensson, and L.G. Johansson, KCl-Induced High Temperature Corrosion of the Austenitic Fe-Cr-Ni Alloys 304L and Sanicro 28 at 600 °C, *Corros. Sci.*, 2006, **48**(6), p 1368-1378
11. J. Pettersson, H. Asteman, J.E. Svensson, and L.G. Johansson, KCl Induced Corrosion of a 304-Type Austenitic Stainless Steel at 600 °C; the Role of Potassium, *Oxid. Met.*, 2005, **64**(1-2), p 23-41
12. C. Berlanga and J.A. Ruiz, Study of Corrosion in a Biomass Boiler, *J. Chem.*, 2013, **2013**, p 1-8
13. Y. Kawahara, Application of High Temperature Corrosion-Resistant Materials and Coatings Under Severe Corrosive

- Environment in Waste-to-Energy Boilers, *J. Therm. Spray Technol.*, 2007, **16**(2), p 202-213
14. R. Bender and M. Schütze, The Role of Alloying Elements in Commercial Alloys for Corrosion Resistance in Oxidizing-Chloridizing Atmospheres Part I: Literature Evaluation and Thermodynamic Calculations on Phase Stabilities, *Mater. Corros.*, 2003, **54**(8), p 567-586
 15. E.O. Ezugwu, Z.M. Wang, and A.R. Machado, The Machinability of Nickel-Based Alloys: A Review, *J. Mater. Process. Technol.*, 1999, **86**(1-3), p 1-16
 16. L. Pawlowski, *The Science and Engineering of Thermal Spray Coatings*, John Wiley & Sons, 2008
 17. M. Oksa, J. Metsäjoki, and J. Kärki, Thermal Spray Coatings for High-Temperature Corrosion Protection in Biomass Co-Fired Boilers, *J. Therm. Spray Technol.*, 2014, **24**(1-2), p 194-205
 18. S. Tuurna, T. Varis, K. Penttilä, K. Ruusuvoori, S. Holmström, and S. Yli-Olli, Optimised Selection of New Protective Coatings for Biofuel Boiler Applications, *Mater. Corros.*, 2011, **62**(7), p 642-649
 19. T. Varis et al., High Temperature Corrosion of Thermally Sprayed NiCr and FeCr Coatings Covered with a KCl-K₂SO₄ Salt Mixture, *Surf. Coat. Technol.*, 2015, **265**, p 235-243
 20. T. Hussain, T. Dudziak, N.J. Simms, and J.R. Nicholls, Fireside Corrosion Behavior of HVOF and Plasma-Sprayed Coatings in Advanced Coal/Biomass Co-fired Power Plants, *J. Therm. Spray Technol.*, 2013, **22**(5), p 797-807
 21. M.A. Uusitalo, P.M.J. Vuoristo, and T.A. Mäntylä, High Temperature Corrosion of Coatings and Boiler Steels Below Chlorine-Containing Salt Deposits, *Corros. Sci.*, 2004, **46**(6), p 1311-1331
 22. M. Uusitalo, P.M. Vuoristo, and T. Mäntylä, High Temperature Corrosion of Coatings and Boiler Steels in Oxidizing Chlorine-Containing Atmosphere, *Mater. Sci. Eng. A*, 2003, **346**(1-2), p 168-177
 23. G. Bolelli et al., Tribological Behavior of HVOF- and HVAF-Sprayed Composite Coatings Based on Fe-Alloy + WC-12% Co, *Surf. Coat. Technol.*, 2014, **248**, p 104-112
 24. A.P. Wang, T. Zhang, and J.Q. Wang, Formation and Properties of Ni-Based Amorphous Metallic Coating Produced by HVAF Thermal Spraying, *Mater. Trans.*, 2005, **46**(5), p 1010-1015
 25. A. Verstak and V. Baranovski, Activated Combustion HVAF Coatings for Protection against Wear and High Temperature Corrosion, *Therm. Spray 2003 Adv. Sci. Appl. Technol.*, 2003, p 535-541
 26. E. Sadeghimeresht, N. Markocsan, P. Nylén, and S. Björklund, Corrosion Performance of Bi-Layer Ni/Cr₂C₃-NiCr HVAF Thermal Spray Coating, *Appl. Surf. Sci.*, 2016, **369**, p 470-481
 27. A. Verstak, High Velocity Air-Fuel Spraying and Its Applications in Oil and Gas Industry, California, 2012.
 28. C. Lyphout et al., Tribological Properties of Hard Metal Coatings Sprayed by High-Velocity Air Fuel Process, *J. Therm. Spray Technol.*, 2016, **25**(1-2), p 331-345
 29. A. Milanti, V. Matikainen, H. Koivuluoto, G. Bolelli, L. Lusvarghi, and P. Vuoristo, Effect of Spraying Parameters on the Microstructural and Corrosion Properties of HVAF-Sprayed Fe-Cr-Ni-B-C Coatings, *Surf. Coat. Technol.*, 2015, **277**, p 81-90
 30. E. Sadeghimeresht, H. Hooshyar, N. Markocsan, S. Joshi, and P. Nylén, Oxidation Behavior of HVAF-Sprayed NiCoCrAlY Coating in H₂-H₂O Environment, *Oxid. Met.*, 2016, **86**(3-4), p 299-314
 31. G. Wang, Z. Huang, P. Xiao, and X. Zhu, Spraying of Fe-Based Amorphous Coating with High Corrosion Resistance by HVAF, *J. Manuf. Process.*, 2016, **22**, p 34-38
 32. E. Sadeghimeresht, N. Markocsan, M. Huhtakangas, and S. Joshi, Isothermal Oxidation of HVAF-Sprayed Ni-Based Chromia, Alumina and Mixed-Oxide Scale Forming Coatings in Ambient Air, *Surf. Coat. Technol.*, 2017, **316**, p 10-21
 33. R. Bender and M. Schütze, The Role of Alloying Elements in Commercial Alloys for Corrosion Resistance in Oxidizing-Chloridizing Atmospheres. Part II: Experimental Investigations, *Mater. Corros.*, 2003, **54**(9), p 652-686
 34. N. Bala, H. Singh, S. Prakash, and J. Karthikeyan, Investigations on the Behavior of HVOF and Cold Sprayed Ni-20Cr Coating on T22 Boiler Steel in Actual Boiler Environment, *J. Therm. Spray Technol.*, 2012, **21**(1), p 144-158
 35. M.H. Enayati, F. Karimzadeh, M. Tavoosi, B. Movahedi, and A. Tahvilian, Nanocrystalline NiAl Coating Prepared by HVOF Thermal Spraying, *J. Therm. Spray Technol.*, 2011, **20**(3), p 440-446
 36. Y.S. Li, Y. Niu, and M. Spiegel, High Temperature Interaction of Al/Si-Modified Fe-Cr Alloys with KCl, *Corros. Sci.*, 2007, **49**(4), p 1799-1815
 37. K.N. Strafford, P.K. Datta, and G. Forster, High-Temperature Chloridation of Binary FeCr Alloys at 1000 °C, *Mater. Sci. Eng. A*, 1989, **120-121**(PART 1), p 61-68
 38. T.S. Sidhu, A. Malik, S. Prakash, and R.D. Agrawal, Cyclic Oxidation Behavior of Ni- and Fe-Based Superalloys in Air and Na 2 SO 4-25% NaCl Molten Salt Environment at 800 °C, *Int. J. Phys. Sci.*, 2006, **1**(September), p 27-33
 39. T. Jonsson, A. Slomian, T.N. Lomholt, S. Kiamehr, and K.V. Dahl, Microstructural Investigations of Pure Nickel Exposed to KCl Induced High Temperature Corrosion, *Mater. High Temp.*, 2015, **32**(1-2), p 44-49
 40. T.J. Pan, Y.S. Li, Q. Yang, R.F. Feng, and A. Hirose, Internal Oxidation and Phase Transformations of Multi-phase Fe-Ni-Al and Fe-Ni-Al-Cr Alloys Induced by KCl Corrosion, *Corros. Sci.*, 2011, **53**(6), p 2115-2121
 41. Y.S. Li and M. Spiegel, Models Describing the Degradation of FeAl and NiAl Alloys Induced by ZnCl₂/KCl Melt at 400-450 °C, *Corros. Sci.*, 2004, **46**(8), p 2009-2023
 42. C.J. Wang and C.C. Li, Corrosion Behaviors of AISI, 1025 Steels with Electroless Nickel/Aluminized Coatings in NaCl-Induced Hot Corrosion, *Surf. Coat. Technol.*, 2004, **177-178**, p 37-43
 43. F.H. Yuan, Z.X. Chen, Z.W. Huang, Z.G. Wang, and S.J. Zhu, Oxidation Behavior of Thermal Barrier Coatings with HVOF and Detonation-Sprayed NiCrAlY Bondcoats, *Corros. Sci.*, 2008, **50**(6), p 1608-1617
 44. B. Wang, J. Gong, A.Y. Wang, C. Sun, R.F. Huang, and L.S. Wen, Oxidation Behaviour of NiCrAlY Coatings on Ni-Based Superalloy, *Surf. Coat. Technol.*, 2002, **149**(1), p 70-75